Performance Analysis and Comparison of Clipped and Filtered OFDM Systems With Iterative Distortion Recovery Techniques

Ying Sun and Hideki Ochiai, *Senior Member, IEEE*

***Abstract*— A well-known drawback of orthogonal frequency-division multiplexing (OFDM) is its signal with high peak-to-average power ratio (PAPR). Among a number of PAPR reduction techniques, clipping and filtering (CAF) is the simplest approach, which effectively reduces the PAPR of band-limited OFDM signals at the cost of increasing in-band distortion. In order to mitigate the performance degradation caused by the in-band distortion, several iterative distortion recovery techniques have been proposed in the literature, and they are largely classified into time-domain (TD) and frequency-domain (FD) compensation approaches: The former and latter are represented by the decision-aided reconstruction (DAR) and clipping noise cancellation (CNC), respectively. To date, however, their theoretical performance limits have not been studied. In this work, we revisit the performance limits of CAF and derive a closed-form signal-to-distortion power ratio (SDR) expression. Furthermore, we introduce a time-domain distortion model for characterizing the OFDM signal with CAF, based on which we make performance comparison between the two compensation approaches. Theoretical analysis and simulations in terms of their achievable symbol error rate (SER) reveal that, unlike the FD counterpart, the TD compensation may suffer from unrecoverable distortion when filtering after clipping is applied at the transmitter.**

***Index Terms*— Clipping and filtering (CAF), clipping noise cancellation (CNC), decision-aided reconstruction (DAR), orthogonal frequency-division multiplexing (OFDM).**

I. Introduction

ORTHOGONAL frequency-division multiplexing (OFDM) signaling has been widely accepted due to its significant advantages over conventional single-carrier systems such as high bandwidth efficiency and robustness against frequency-selective fading channels with low-complexity receiver structure based on cyclic prefix (CP). However, one of the critical disadvantages in view of its practical implementation is the resulting signal with high peak-to-average power ratio (PAPR), which leads to considerable penalty in terms of achievable power amplifier efficiency at the transmitter.

A number of PAPR reduction techniques have been proposed for OFDM systems, which are summarized in, e.g., [1], [2]. Among many approaches, this paper focuses on clipping and filtering (CAF) [3], [4], as it is applicable to most OFDM systems without major modification in principle. CAF is the simplest and straightforward approach which causes neither average power increase nor bandwidth expansion in order to reduce PAPR. Furthermore, the increase in terms of transmitter complexity may not be significant compared to other schemes involving some optimization processes. Compared to simple clipping of OFDM samples [5], by performing clipping on the oversampled OFDM signals and then filtering out the out-of band (OOB) distortion, it can not only reduce PAPR effectively, but also increase the achievable signal-to-distortion power ratio (SDR) [4]. Similar approaches include peak cancellation [6], which trades off the distortion and OOB radiation by intentionally adding the time-domain canceling peaks, and its performance analysis can be found in [7].

Apparently, the most critical issue of CAF is its residual clipping distortion that falls within the signal bandwidth. Since the distortion (or clipping noise) caused by CAF depends on the transmit signal waveform, the simple conventional receiver that assumes the distortion to be Gaussian independent of the input signal is sub-optimal. On the other hand, the complexity of optimal receivers, such as those based on maximum-likelihood detection principle [8]–[10] should be prohibitive in practice. In the literature, several low-complexity iterative distortion recovery techniques have been proposed, and they are largely categorized into the two approaches: time-domain (TD) and frequency-domain (FD) compensation. The former is represented by the decision-aided reconstruction (DAR) [11], whereas the latter is well known as the clipping noise cancellation (CNC) [12]. The TD approach attempts to reconstruct the clipped signal based on the fact that the original peak envelope may be above the clipping level, whereas the FD approach attempts to cancel the clipping noise on each subcarrier based on the signal model resulting from Bussgang's theorem [13].

In this work, we focus on comparing the achievable performance of the above-mentioned two clipping recovery approaches for OFDM systems. In particular, we introduce

Manuscript received November 24, 2020; revised March 11, 2021; accepted May 16, 2021. Date of publication June 2, 2021; date of current version November 11, 2021. This work was supported in part by MIC/SCOPE under Grant 205003001 and in part by the Japan Society for the Promotion of Science (JSPS) through the Grants-in-Aid for Scientific Research (KAKENHI) under Grant 21H04873. The associate editor coordinating the review of this article and approving it for publication was X. Yuan. *(Corresponding author: Hideki Ochiai.)*

The authors are with the Department of Electrical and Computer Engineering, Yokohama National University, Yokohama 240-8501, Japan (e-mail: sun-ying-kz@ynu.jp; hideki@ynu.ac.jp).

Color versions of one or more figures in this article are available at https://doi.org/10.1109/TWC.2021.3083537.

Digital Object Identifier 10.1109/TWC.2021.3083537

a new analytical model of OFDM systems with CAF suitable for analyzing time-domain distortion compensation approach, and theoretically derive a closed-form upper bound on its achievable signal-to-noise plus distortion ratio (SNDR). Recent studies on clipping recovery techniques for OFDM include those based on compressed sensing [14]–[17], which may offer a better trade-off in terms of complexity and achievable performance compared to the pioneering work [11], [12]. Our results may also serve as performance bounds for these schemes depending on whether the compensation is performed based on TD or FD model.

Throughout the paper, we focus on the fundamental performance of the uncoded OFDM system over both additive white Gaussian noise (AWGN) and frequency-selective Rayleigh fading channels. Our analytical results on SNDR may be also valid for *coded* OFDM systems (e.g., [18]–[21]), but their precise analysis is beyond the scope of this work. We note that most of the conventional TD compensation schemes such as the original work of DAR [11] as well as [14], [16], [18], [19], [21] have been focused on the clipped OFDM signal (without filtering), but as mentioned above, clipping should be applied to oversampled OFDM signals together with filtering for lower PAPR and higher SDR. It will be shown that in the presence of CAF, the TD reconstruction process fails to take into account the effect of filtering on the resulting signals and thus should lead to some degradation in terms of its achievable performance.

The main contributions of this work are summarized as follows: 1) We revisit the performance of OFDM system with CAF and develop a simple closed-form SNDR expression that can be approached by OFDM with a large number of subcarriers and oversampling factor. An expression for symbol error rate (SER) lower bound is also derived. 2) A new time-domain analytical model for the distortion associated with CAF is introduced, based on which the upper bound of SNDR for the receiver with TD signal reconstruction is developed. Furthermore, the upper bound of SNDR achieved by the ideal FD distortion cancellation is also derived. 3) We make a comparative study on DAR (as a TD compensation representative) and CNC (as a FD compensation representative) over AWGN and Rayleigh fading channels through extensive simulations and reveal the superiority of CNC compared to DAR in the presence of CAF at the transmitter, which is supported by their corresponding theoretical performance bounds.

The remainder of this paper is organized as follows. Section II describes the OFDM transmission system with CAF process as well as the two representative clipping distortion recovery techniques (i.e., DAR and CNC) for later simulations. A new closed-form SNDR expression as well as SER lower bound for the OFDM system with CAF are developed in Section III. An upper bound of the achievable SNDR performance by the ideal TD compensation approach is derived based on a new time-domain analytical distortion model in Section IV, together with that by the ideal FD compensation approach. Simulation results in terms of the achievable SER with high-order modulations that justify our findings in this work are presented in Section V. Finally, concluding remarks are given in Section VI.

Notation: Since this paper frequently refers to the time-domain samples as well as their frequency-domain counterparts, for the sake of readability, the capital letters such as X and Y will be consistently used for the variables in the frequency domain, whereas their lower-case counterparts such as x and y are reserved for the time-domain variables. The same rule applies to their vector representations given in the bold-face letters.

II. System Description

In this section, we first describe the OFDM system model with CAF followed by the iterative distortion cancellation receivers considered throughout this paper.

A. OFDM Transmitter With CAF

We consider an N-subcarrier OFDM system where each subcarrier is modulated by M^2-ary quadrature amplitude modulation (QAM). Specifically, let $\mathcal{X} \subset \mathbb{R}$ denote a set of an M-ary pulse amplitude modulation (PAM) constellation points. Then, the set of square M^2-ary QAM constellation points $\mathcal{Z}$ is expressed by $\mathcal{Z} = \mathcal{X}^2 \subset \mathbb{C}$. A set of N QAM symbols, denoted by $\mathbf{Z} = (Z_0, Z_1, \ldots, Z_{N-1}) \in \mathcal{Z}^N$, is carried by a single N-subcarrier OFDM symbol after clipping and filtering (CAF). The QAM symbol on the kth subcarrier is given by $Z_k = X_k + jY_k$ with $X_k, Y_k \in \mathcal{X}$ for $k \in \{0, 1, \ldots, N-1\}$. We also assume that $\{X_k\}$ and $\{Y_k\}$ are independent and identically distributed (i.i.d.) M-ary PAM symbols with $\Pr(X_k = X) = \Pr(Y_k = X) = 1/M$ for any $X \in \mathcal{X}$ and subcarrier index k. The average power of the OFDM signal before CAF can be defined as $P_{\text{in}} \triangleq \frac{1}{N} E\left\{\|\mathbf{Z}\|^2\right\}$, where $E\{\cdot\}$ denotes expectation.

In order to effectively reduce the peak power of OFDM signals, the clipping operation should be performed on an oversampled version of OFDM symbols [4]. Following [4], we first generate the J-times oversampled time-domain OFDM signal by JN-point inverse discrete Fourier transform (IDFT) denoted by $\mathbf{z} = (z_0, z_1, \ldots, z_{JN-1}) \in \mathbb{C}^{JN}$, where

$$z_\ell = \frac{1}{\sqrt{N}} \sum_{k=0}^{N-1} Z_k e^{j2\pi \frac{k}{JN}\ell}, \quad \ell = 0, 1, \ldots, JN-1. \tag{1}$$

Provided that the product JN is chosen as an integer power of 2, the above process can be efficiently implemented by JN-point inverse fast Fourier transform (IFFT) after appending $(J-1)N$ zeros to $\mathbf{Z}$, i.e.,

$$\mathbf{z} = \sqrt{J}\,\mathrm{IFFT}_{JN}\left(\mathbf{Z}'\right), \qquad \mathbf{Z}' \triangleq \left(\mathbf{Z}, \mathbf{0}_{(J-1)N}\right), \tag{2}$$

where $\mathbf{0}_n$ denotes the all-zero vector of length n.[1]

The samples output from the IFFT process are then clipped by soft-envelope limiter, and the resulting signal samples are given by $\tilde{\mathbf{z}} = (\tilde{z}_0, \tilde{z}_1, \ldots, \tilde{z}_{JN-1}) \in \mathbb{C}^{JN}$, where

$$\tilde{z}_\ell = \begin{cases} z_\ell, & \text{for } |z_\ell| \le A, \\ Ae^{j \arg z_\ell}, & \text{for } |z_\ell| > A, \end{cases} \tag{3}$$

[1]The oversampling factor J need not be necessarily an integer, as long as JN is an integer power of 2. However, in this work we restrict our attention to the case with $J = 2^\ell$, $\ell = 1, 2, \ldots$, for simplicity.

with A representing the maximum envelope level over which the signal envelope is clipped. We define the clipping ratio γ as [4]

$$\gamma = \frac{A}{\sqrt{P_{\rm in}}}. \tag{4}$$

Due to oversampling, the clipping process will generate OOB distortion components, which should be removed by filtering operation. Specifically, after JN-point FFT of clipped signal samples $\tilde{\mathbf{z}}$, we have $\mathbf{U}' \triangleq (\mathbf{U}, \mathbf{U}_{\rm OOB})$ with $\mathbf{U} = (U_0, U_1, \ldots, U_{N-1}) \in \mathbb{C}^N$ and $\mathbf{U}_{\rm OOB} = (U_N, U_{N+1}, \ldots, U_{JN-1}) \in \mathbb{C}^{(J-1)N}$ representing the in-band and out-of-band components, respectively, where

$$U_k = \frac{1}{\sqrt{JN}} \sum_{\ell=0}^{JN-1} \tilde{z}_\ell e^{-j2\pi \frac{k}{JN}\ell},\ k = 0, 1, \ldots, JN-1. \tag{5}$$

We define the corresponding output power as $P_{\rm out} \triangleq \frac{1}{N} E\left\{\|\mathbf{U}'\|^2\right\}$, and by the assumption of OFDM signal as Gaussian, it follows that $P_{\rm out} = (1 - e^{-\gamma^2}) P_{\rm in}$ [4]. Due to the signal bandwidth constraint, $\mathbf{U}_{\rm OOB}$ should be removed before transmission.

The resulting signal with J-times oversampling after CAF, denoted by $\mathbf{u} \in \mathbb{C}^{JN}$, is expressed, similar to (2), as

$$\mathbf{u} = \sqrt{J}\,\mathrm{IFFT}_{JN}(\mathbf{U}''), \qquad \mathbf{U}'' \triangleq \left(\mathbf{U}, \mathbf{0}_{(J-1)N}\right). \tag{6}$$

Note that the average power of the transmitted signal is reduced from the original input vector due to the clipping and filtering process, and this reduction factor can be defined as

$$\eta \triangleq \frac{E\left\{\|\mathbf{U}\|^2\right\}}{E\left\{\|\mathbf{Z}\|^2\right\}} = \frac{E\left\{\|\mathbf{U}\|^2\right\}}{NP_{\rm in}}. \tag{7}$$

The OFDM signal thus generated is then followed by an addition of cyclic prefix (CP) and is transmitted over frequency-selective Rayleigh fading channels. It should be noted that the signal representation of (6) does not take into account the appropriate frequency offset [4] that is required in practice so as to make the power spectrum symmetric, as it does not affect our subsequent analysis based on the baseband signal model.

At the receiver, assuming that the CP length is larger than or equal to the effective impulse response length of channel such that the inter-symbol interference (ISI) can be avoided, the received signal in the frequency domain obtained by CP removal and N-point FFT will be expressed as $\mathbf{V} = (V_0, V_1, \ldots, V_{N-1}) \in \mathbb{C}^N$ with

$$V_k = H_k U_k + W_k, \tag{8}$$

where $H_k \in \mathbb{C}$ and $W_k \in \mathbb{C}$ are the frequency response of the channel and AWGN term corresponding to the kth subcarrier, respectively. Note that increasing CP length will reduce spectral efficiency, but it does not affect our result on SER performance. We may express

$$\mathbf{V}^T = \mathbf{H}\,\mathbf{U}^T + \mathbf{W}^T, \tag{9}$$

where $\mathbf{H} = \mathrm{diag}(H_0, H_1, \ldots, H_{N-1}) \in \mathbb{C}^{N\times N}$ is the diagonal matrix formed by the channel coefficients H_k, and $\mathbf{W} = (W_0, W_1, \ldots, W_{N-1}) \in \mathbb{C}^N$ is the AWGN vector with each of the noise components W_k following the i.i.d. circularly symmetric complex Gaussian distribution with zero mean and variance $P_n \triangleq E\left\{|W_k|^2\right\}$, i.e., $W_k \sim \mathcal{CN}(0, P_n)$.

Assuming the perfect knowledge of $\mathbf{H}$, after zero-forcing (ZF) equalization at the receiver for fading channel compensation, we obtain

$$\tilde{\mathbf{Z}}^T = \mathbf{H}^{-1}\mathbf{V}^T = \mathbf{U}^T + \underbrace{\mathbf{H}^{-1}\mathbf{W}^T}_{\triangleq \mathbf{W}'^T}, \tag{10}$$

where $\tilde{\mathbf{Z}} = \left(\tilde{Z}_0, \tilde{Z}_1, \ldots, \tilde{Z}_{N-1}\right)$ corresponds to the vector representing the received (noisy) QAM symbol and the kth element of $\mathbf{W}'$ follows $W'_k \sim \mathcal{CN}(0, P_n/\zeta_k)$ for $\zeta_k \triangleq |H_k|^2$.

Note that based on Bussgang's theorem [13], the received clipped and filtered symbol vector after ZF equalization may be expressed as

$$\tilde{\mathbf{Z}} = \underbrace{\alpha\mathbf{Z} + \mathbf{D}}_{\triangleq \mathbf{U}} + \mathbf{W}', \tag{11}$$

where, under the assumption of Gaussian process of OFDM signals, the attenuation factor $\alpha \in \mathbb{R}$ is expressed as [4], [13]

$$\alpha = 1 - e^{-\gamma^2} + \tfrac{\sqrt{\pi}\gamma}{2}\mathrm{erfc}(\gamma), \tag{12}$$

and $\mathbf{D} = (D_0, D_1, \ldots, D_{N-1}) \in \mathbb{C}^N$ is the in-band distortion component.

B. PAM Detection

At the receiver, the hard decision is made for real and imaginary parts of $\tilde{\mathbf{Z}}$ independently based on one-dimensional PAM detection, considering the effect of the scaling factor due to CAF. For a set of PAM points $X \in \mathcal{X}$ used at the transmitter, the detector should replace it by αX, or the received symbol should be scaled by $1/\alpha$ before the hard decision is made based on $\mathcal{X}$. Let $\hat{Z}_k = \hat{X}_k + j\hat{Y}_k$ denote the estimated symbol for a given received symbol $\tilde{Z}_k = \tilde{X}_k + j\tilde{Y}_k$. The PAM detector will make hard decision on $\tilde{X}_k$ according to:

$$\hat{X}_k = \arg\min_{X\in\mathcal{X}} \left|X - \tilde{X}_k/\alpha\right|^2. \tag{13}$$

The hard decision on $\hat{Y}_k$ is performed in the same manner.

C. Signal-to-Noise Power Ratio

The average signal power after CAF can be expressed using (7) as

$$P_{\rm av} = \frac{1}{N} E\left\{\|\mathbf{U}\|^2\right\} = \eta P_{\rm in} \tag{14}$$

and the signal-to-noise power ratio (SNR) is defined as

$$\mathrm{SNR} \triangleq \frac{P_{\rm av}}{P_n} = \eta\frac{P_{\rm in}}{P_n}. \tag{15}$$

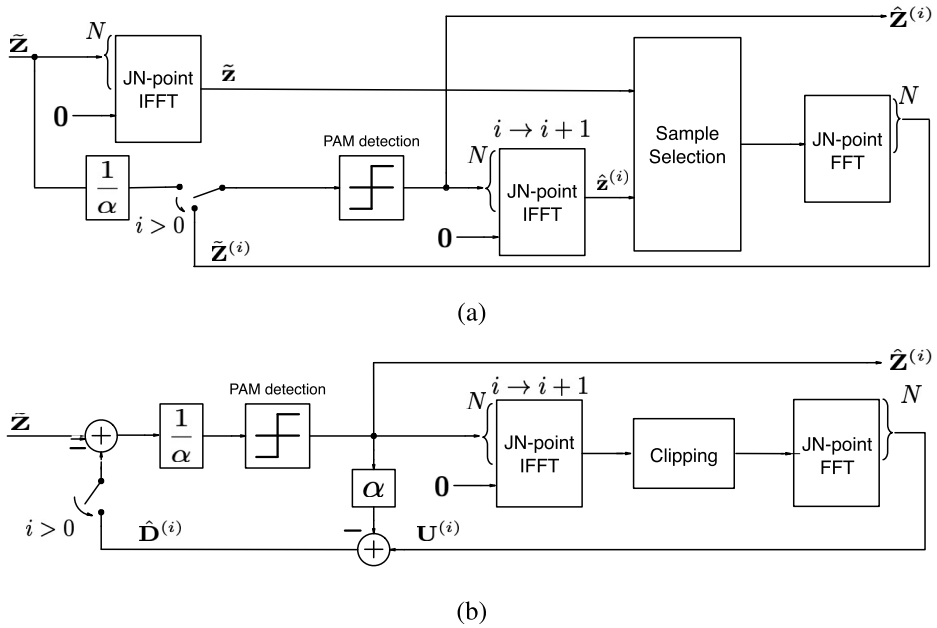

Fig. 1. Block diagrams of (a) DAR and (b) CNC.

D. Distortion Recovery Approaches

In principle, the in-band distortion components $\mathbf{D}$ generated by the clipping process are statistically dependent on the transmit symbols $\mathbf{Z}$, and thus treating $\mathbf{D}$ as Gaussian noise independent of $\mathbf{Z}$, as assumed in [4], would result in sub-optimal detection. The optimal maximum-likelihood detection (see, e.g., [9], [10]), however, would lead to the receiver complexity of exponential order with N. Therefore, sub-optimal iterative recovery procedures are usually adopted. One would apply either a time-domain approach that attempts to reconstruct the unclipped signal z_ℓ from $\tilde{z}_\ell$ according to the clipping process of (3), or a frequency-domain approach that estimates the distortion term $\mathbf{D}$ observed in the QAM symbols according to (11). The pioneering work based on the former approach is the decision-aided reconstruction (DAR) [11], whereas that based on the latter approach is the clipping noise cancellation (CNC) [12]. The entire block diagrams of DAR and CNC designed for our OFDM system model with CAF are shown in Figs. 1 (a) and (b), respectively, which we briefly review in what follows.

1) Decision-Aided Reconstruction: When CAF is applied at the transmitter and the receiver performs sampling of the received OFDM signal at Nyquist rate (i.e., without over-sampling), DAR should regenerate the oversampled version of the received signals: For a given received vector $\tilde{\mathbf{Z}}$ after ZF equalization by (10), the OFDM symbol is zero padded and then converted to the time-domain symbols by JN-point IFFT to reproduce the oversampled clipped and filtered OFDM signal denoted by $\tilde{\mathbf{z}} = (\tilde{z}_0, \tilde{z}_1, \ldots, \tilde{z}_{JN-1}) \in \mathbb{C}^{JN}$, where

$$\tilde{\mathbf{z}} = \sqrt{J}\,\mathrm{IFFT}_{JN}\left(\tilde{\mathbf{Z}}'\right), \qquad \tilde{\mathbf{Z}}' \triangleq \left(\tilde{\mathbf{Z}}, \mathbf{0}_{(J-1)N}\right), \quad (16)$$

$$= \mathbf{u} + \mathbf{w}' \quad (17)$$

with $\mathbf{u}$ given by (6) and $\mathbf{w}' \in \mathbb{C}^{JN}$ representing an AWGN vector after ZF equalization.

By assuming that the receiver has knowledge of clipping ratio γ applied at the transmitter, the DAR algorithm for the case of CAF may be described as follows:

i) From $\tilde{\mathbf{Z}}$ in (11), generate an oversampled reference signal $\tilde{\mathbf{z}}$ according to (16).

ii) By applying hard decision to $\tilde{\mathbf{Z}}/\alpha$, obtain the initial estimate of $\mathbf{Z}$, denoted by $\hat{\mathbf{Z}}^{(0)} = \left(\hat{Z}_0^{(0)}, \hat{Z}_1^{(0)}, \ldots, \hat{Z}_{N-1}^{(0)}\right) \in \mathcal{Z}^N$. Set the iteration counter by $i = 1$.

iii) For the ith iteration, using the previously detected symbol vector $\hat{\mathbf{Z}}^{(i-1)} \in \mathcal{Z}^N$, reproduce the time-domain oversampled OFDM symbol through JN-point IFFT, which is denoted by $\hat{\mathbf{z}}^{(i-1)} = \left(\hat{z}_0^{(i-1)}, \hat{z}_1^{(i-1)}, \ldots, \hat{z}_{JN-1}^{(i-1)}\right) \in \mathbb{C}^{JN}$.

iv) The DAR detector will output the OFDM samples $\hat{\mathbf{z}}^{(i)} = \left(\hat{z}_0^{(i)}, \hat{z}_1^{(i)}, \ldots, \hat{z}_{JN-1}^{(i)}\right) \in \mathbb{C}^{JN}$ according to

$$\hat{z}_\ell^{(i)} = \begin{cases} \tilde{z}_\ell, & \text{if } \left|\hat{z}_\ell^{(i-1)}\right| \le A, \\ \hat{z}_\ell^{(i-1)}, & \text{if } \left|\hat{z}_\ell^{(i-1)}\right| > A, \end{cases} \quad (18)$$

for $\ell = 0, 1, \ldots, JN-1$. The time-domain samples $\hat{\mathbf{z}}^{(i)}$ are converted to the frequency domain samples by JN-point FFT and then the first N in-band subcarriers are selected as $\tilde{\mathbf{Z}}^{(i)} = \left(\tilde{Z}_0^{(i)}, \tilde{Z}_1^{(i)}, \ldots, \tilde{Z}_{N-1}^{(i)}\right) \in \mathbb{C}^N$.

v) By applying hard decision to $\tilde{\mathbf{Z}}^{(i)}$ (without scaling by $1/\alpha$), obtain the revised estimate $\hat{\mathbf{Z}}^{(i)} = \left(\hat{Z}_0^{(i)}, \hat{Z}_1^{(i)}, \ldots, \hat{Z}_{N-1}^{(i)}\right) \in \mathcal{Z}^N$.

vi) If i reaches the predetermined iteration limit $I_{\max}$, output $\hat{\mathbf{Z}}^{(I_{\max})}$ and stop. Otherwise, increment the counter i by 1 and go to Step iii).

2) Clipping Noise Cancellation: The CNC algorithm of [12] is described as follows:

i) By applying hard decision to $\tilde{\mathbf{Z}}/\alpha$ in (11), obtain the initial estimate of $\mathbf{Z}$, denoted by $\hat{\mathbf{Z}}^{(0)} = \left(\hat{Z}_0^{(0)}, \hat{Z}_1^{(0)}, \ldots, \hat{Z}_{N-1}^{(0)}\right) \in \mathcal{Z}^N$. Set the iteration counter by $i = 1$.

ii) For the ith iteration, using the previously detected symbol vector $\hat{\mathbf{Z}}^{(i-1)} \in \mathcal{Z}^N$, perform the same CAF process as in the transmitter side. Let $\mathbf{U}^{(i)} = \left(U_0^{(i)}, U_1^{(i)}, \ldots, U_{N-1}^{(i)}\right) \in \mathbb{C}^N$ denote the resulting symbol vector.

iii) Estimate the distortion vector by

$$\hat{\mathbf{D}}^{(i)} = \mathbf{U}^{(i)} - \alpha\hat{\mathbf{Z}}^{(i-1)}, \tag{19}$$

and subtract this from the received vector. It generates

$$\tilde{\mathbf{Z}}^{(i)} = \tilde{\mathbf{Z}} - \hat{\mathbf{D}}^{(i)}. \tag{20}$$

iv) By applying hard decision to $\tilde{\mathbf{Z}}^{(i)}/\alpha$, obtain the revised estimate $\hat{\mathbf{Z}}^{(i)} = \left(\hat{Z}_0^{(i)}, \hat{Z}_1^{(i)}, \ldots, \hat{Z}_{N-1}^{(i)}\right) \in \mathcal{Z}^N$.

v) If i reaches the predetermined iteration limit $I_{\max}$, output $\hat{\mathbf{Z}}^{(I_{\max})}$ and stop. Otherwise, increment the counter i by 1 and go to Step ii).

3) Complexity Comparison: From Fig. 1, we observe that each iteration for clipping distortion estimation and recovery process needs a pair of IFFT and FFT, and thus the complexity order of both approaches is the same, i.e., $O(JN \log_2 JN)$ per iteration. In the case of DAR for the OFDM with CAF, the initial reconstruction of the oversampled signal according to (16) is necessary, which requires an additional operation of IFFT as shown in Fig. 1(a). The overall complexity depends largely on the number of iterations that would be required for each scheme to achieve a target error performance. This will be investigated in Section V.

III. Asymptotic SDR Analysis of Clipped and Filtered OFDM Signals

In this section, we revisit the performance analysis of clipped and filtered OFDM signals. Specifically, we develop an SDR expression of clipped and filtered OFDM signals based on the classical analysis on nonlinear transformation of Gaussian processes [22], assuming that OFDM signal is modeled by a band-limited complex Gaussian random process following [23], [24]. Furthermore, we derive a simple SER lower bound that serves as a benchmark of the OFDM with CAF (Theorem 1). To the best of the authors' knowledge, the application of such a theoretical framework to the SER performance evaluation of the OFDM signals with CAF has not been considered before.

In [4], a different analytical method has been developed that can numerically calculate the distortion components of each subcarrier for a given clipping ratio γ and oversampling factor J. The resulting SDR expression derived by this approach is summarized in Appendix, where it is revealed that our simpler analytical expression developed in this section may serve as an asymptotic limit for clipped and filtered OFDM signals with a large number of subcarriers and sufficiently high oversampling factor.

A. Power Spectral Density of Complex Gaussian Process With Soft-Envelope Limiter

With reference to (3), let $z(t)$ denote a complex Gaussian random process that will be input to the soft-envelope limiter and $\tilde{z}(t)$ denote its output. The power spectral density (PSD) of $\tilde{z}(t)$, $S_{\tilde{z}}(f)$, can be expressed as [24, Eq.(19)]

$$S_{\tilde{z}}(f) = P_{\text{in}} \sum_{n=0}^{\infty} \frac{C_n}{P_{\text{in}}^{2n+1}} S_z^{\star(2n+1)}(f), \tag{21}$$

where $S_z(f)$ is the PSD of the input $z(t)$ and $S_z^{\star(m)}(f)$ is the m-fold convolution of $S_z(f)$ with itself, i.e.,

$$S_z^{\star(m)}(f) = \underbrace{S_z(f) \star \cdots \star S_z(f)}_{m}, \tag{22}$$

for $m > 1$ and $S_z^{\star(1)}(f) = S_z(f)$, with $\star$ representing convolution operation. By definition, the average power of the output signal is given by

$$P_{\text{out}} = \int_{-\infty}^{\infty} S_{\tilde{z}}(f) df, \tag{23}$$

and the PSD of input signal should satisfy the following relationship for any positive integer m:

$$\int_{-\infty}^{\infty} S_z^{\star(m)}(f) df = P_{\text{in}}^m. \tag{24}$$

The coefficient C_n in (21) depends on the nonlinear function and in the case of soft-envelope limiter, it can be expressed as[2] (25), shown at the bottom of the page, where $\text{erfc}(\cdot)$ is the complementary error function,

$$(x)_l = \prod_{i=0}^{l-1} (x + i) \tag{26}$$

is the Pochhammer symbol [25] defined for $x \in \mathbb{R}$ and $l \in \mathbb{N}$, and

$$F_k \triangleq \prod_{m=0}^{k} \frac{2m+1}{2m+2}. \tag{27}$$

[2]This expression is derived in [24, Eq.(27)] with some notational error, which is corrected in this paper.

$$C_n = (n+1)\left| \sum_{k=0}^{n} \binom{n}{k} (-1)^k \left\{ 1 - \left(1 + \sum_{l=1}^{k+1} \left[\frac{1}{l!} - \frac{F_k}{(\frac{1}{2})_l} \right] \gamma^{2l} \right) e^{-\gamma^2} + F_k \sqrt{\pi} \gamma \text{erfc}(\gamma) \right\} \right|^2, \tag{25}$$

TABLE I
NUMERICAL VALUES OF $\delta_{n,\text{in}}$ FOR $n \in [5, 10]$

n	5	6	7	8	9	10
$\delta_{n,\text{in}}$	0.393926	0.365371	0.34224	0.323009	0.306693	0.292623

From (25), C_n consists of linear combinations of terms $\gamma^{2l}e^{-\gamma^2}$ and $\gamma\text{erfc}(\gamma)$ for positive integer l, with the first three coefficients given by

$$\begin{cases} C_0 = \left|1 - e^{-\gamma^2} + \dfrac{\sqrt{\pi}}{2}\gamma\text{erfc}(\gamma)\right|^2 = \alpha^2, \\ C_1 = \dfrac{1}{8}\left|\gamma^2 e^{-\gamma^2} + \dfrac{\sqrt{\pi}}{2}\gamma\text{erfc}(\gamma)\right|^2, \\ C_2 = \dfrac{1}{768}\left|6\gamma^2\, e^{-\gamma^2} - 4\gamma^4\, e^{-\gamma^2} + 3\sqrt{\pi}\gamma\text{erfc}(\gamma)\right|^2. \end{cases} \tag{28}$$

B. Input Signal With Rectangular Spectral Shape

Let us assume that the input signal $z(t)$ is an ideally band-limited Gaussian random process with normalized bandwidth such that its PSD is given by

$$S_z(f) = \begin{cases} P_{\text{in}}, & |f| < \dfrac{1}{2}, \\ 0, & \text{otherwise.} \end{cases} \tag{29}$$

Then, its self-convolution normalized by the input power can be expressed as [26], [27]

$$\begin{aligned} \xi_n(f) &\triangleq \frac{S_z^{\star(2n+1)}(f)}{P_{\text{in}}^{2n+1}} \\ &= (2n+1)\sum_{p=0}^{n-l}\frac{(-1)^p(n+\frac{1}{2}-|f|-p)^{2n}}{p!(2n+1-p)!}, \end{aligned} \tag{30}$$

for

$$\max\left(0, l-\frac{1}{2}\right) < |f| < l+\frac{1}{2}, \tag{31}$$

where $l = 0, 1, \ldots, n$. For example, in the case of $n = 1$ we obtain

$$\xi_1(f) = \frac{S_z^{\star(3)}(f)}{P_{\text{in}}^3} = \begin{cases} \left(\dfrac{3}{4} - |f|^2\right), & |f| < \dfrac{1}{2}, \\ \dfrac{1}{2}\left(\dfrac{3}{2} - |f|\right)^2, & \dfrac{1}{2} < |f| < \dfrac{3}{2}. \end{cases} \tag{32}$$

Furthermore, one can readily calculate $\xi_n(f)$ at $f = 0$, e.g., $\xi_1(0) = \frac{3}{4}$, $\xi_2(0) = \frac{115}{192}$, and $\xi_3(0) = \frac{5887}{11520}$.

C. Output Signal After Filtering

From the above results, the PSD of (21) can be expressed as

$$S_{\tilde{z}}(f) = \alpha^2 S_z(f) + \underbrace{P_{\text{in}}\sum_{n=1}^{\infty} C_n\xi_n(f)}_{\triangleq S_d(f)}, \tag{33}$$

where $S_d(f)$ is the PSD of the distortion term. From (23) and (29), the average power of the distortion term in (33) can be expressed as

$$P_d = \int_{-\infty}^{\infty} S_d(f)df = P_{\text{out}} - \alpha^2 P_{\text{in}}. \tag{34}$$

When the rectangular filtering is applied to the above clipped signal, let $u(t)$ denote its output. The resulting PSD will be expressed from (33) as

$$S_u(f) = \alpha^2 S_z(f) + S_{\hat{d}}(f), \tag{35}$$

where $S_{\hat{d}}(f)$ is the PSD of the distortion term after filtering, which is given by

$$S_{\hat{d}}(f) = \begin{cases} S_d(f), & |f| < \dfrac{1}{2}, \\ 0, & \text{otherwise.} \end{cases} \tag{36}$$

The average power of the distortion that falls within the signal bandwidth is expressed as

$$P_{d,\text{in}} = \int_{-\infty}^{\infty} S_{\hat{d}}(f)df = P_{\text{in}}\sum_{n=1}^{\infty} C_n \underbrace{\int_{-\frac{1}{2}}^{\frac{1}{2}} \xi_n(f)df}_{\triangleq \delta_{n,\text{in}}}, \tag{37}$$

where [24]

$$\begin{aligned} \delta_{n,\text{in}} &= 2\int_0^{\frac{1}{2}} \xi_n(f)df \\ &= 2\sum_{p=0}^{n}(-1)^p\frac{(n-p+\frac{1}{2})^{2n+1} - (n-p)^{2n+1}}{(2n-p+1)!p!}. \end{aligned} \tag{38}$$

As an example, the first several terms of $\delta_{n,\text{in}}$ can be calculated as $\delta_{0,\text{in}} = 1$, $\delta_{1,\text{in}} = \frac{2}{3}$, $\delta_{2,\text{in}} = \frac{11}{20}$, $\delta_{3,\text{in}} = \frac{151}{315}$, and $\delta_{4,\text{in}} = \frac{15\,619}{36\,288}$ [24]. The numerical values of $\delta_{n,\text{in}}$ with $n \in [5, 10]$ are listed in Table I. As a consequence, we may express the power reduction factor η of (7) as

$$\eta = \frac{\alpha^2 P_{\text{in}} + P_{d,\text{in}}}{P_{\text{in}}} = \alpha^2 + \sum_{n=1}^{\infty} C_n\delta_{n,\text{in}} = \sum_{n=0}^{\infty} C_n\delta_{n,\text{in}}. \tag{39}$$

D. Distortion Analysis for OFDM Signals

We now model the PSD of input OFDM signal as defined in (29), which becomes accurate as the number of subcarriers increases and all the subcarriers are assigned with the same input power.

Based on (37), let us define the average signal-to-distortion power ratio (SDR) as

$$\text{SDR}_{\text{av}} \triangleq \frac{\alpha^2 P_{\text{in}}}{P_{d,\text{in}}} = \frac{\alpha^2}{\sum_{n=1}^{\infty} C_n\delta_{n,\text{in}}}, \tag{40}$$

and the SDR observed at frequency f within the signal bandwidth from (33) and (36) as

$$\mathrm{SDR}(f) \triangleq \frac{\alpha^2 P_{\mathrm{in}}}{S_{\hat{d}}(f)} = \frac{\alpha^2}{\sum_{n=1}^{\infty} C_n \xi_n(f)}. \tag{41}$$

Consequently, the signal-to-noise plus distortion ratio (SNDR) observed at frequency f in the case of fading channel with a given squared channel coefficient $\zeta \triangleq |H|^2$ is expressed as

$$\begin{aligned}\mathrm{SNDR}(f;\zeta) &= \frac{\alpha^2 P_{\mathrm{in}}}{P_n/\zeta + S_{\hat{d}}(f)} \\ &= \frac{\alpha^2}{\frac{\eta}{\zeta}\mathrm{SNR}^{-1} + \sum_{n=1}^{\infty} C_n \xi_n(f)}.\end{aligned} \tag{42}$$

Likewise, we may define the average SNDR as

$$\begin{aligned}\mathrm{SNDR}_{\mathrm{av}}(\zeta) &\triangleq \frac{\alpha^2 P_{\mathrm{in}}}{P_n/\zeta + P_{d,\mathrm{in}}} \\ &= \frac{\alpha^2}{\frac{\eta}{\zeta}\mathrm{SNR}^{-1} + \sum_{n=1}^{\infty} C_n \delta_{n,\mathrm{in}}}.\end{aligned} \tag{43}$$

E. Symbol Error Rate Analysis for OFDM Signals

Throughout this work, we evaluate the performance of M-ary PAM for simplicity of analysis and evaluation, while M^2-ary QAM is always transmitted over all the subcarriers as usual. Due to the independence of two PAM symbols, the SER of M-ary PAM, $\mathrm{SER}_{\mathrm{PAM}}$, can be converted to that of the corresponding M^2-ary QAM, $\mathrm{SER}_{\mathrm{QAM}}$, as

$$\mathrm{SER}_{\mathrm{QAM}} = 1 - \left(1 - \mathrm{SER}_{\mathrm{PAM}}\right)^2 \tag{44}$$

for the same value of SNR defined in (15). Assuming that the OFDM signal is modeled as in the previous subsection and the distortion is Gaussian distributed as a result of the central limit theorem, we have the following theorem:

Theorem 1: The symbol error rate (SER) of M-ary PAM signal averaged over all the subcarriers is bounded by

$$\begin{aligned}\mathrm{SER}_{\mathrm{av}} &\geq 2\left(1 - \frac{1}{M}\right) Q\left(\sqrt{\frac{3}{M^2-1}\mathrm{SNDR}_{\mathrm{av}}(\zeta)}\right) \\ &\triangleq \mathrm{SER}_{\mathrm{LB}}(\zeta)\end{aligned} \tag{45}$$

with $Q(x) \triangleq \frac{1}{2}\,\mathrm{erfc}\left(\frac{x}{\sqrt{2}}\right)$, provided that

$$\mathrm{SNDR}(0;\zeta) \geq M^2 - 1. \tag{46}$$

Proof: The SER of M-ary PAM signal over an AWGN channel is given by [28]

$$\begin{aligned}\mathrm{SER} &= 2\left(1 - \frac{1}{M}\right) Q\left(\sqrt{\frac{3}{M^2-1}\mathrm{SNR}}\right) \\ &= \left(1 - \frac{1}{M}\right) \mathrm{erfc}\left(\sqrt{\frac{3}{2(M^2-1)}\mathrm{SNR}}\right).\end{aligned} \tag{47}$$

The assumption that the distortion follows Gaussian distribution allows us to substitute SNDR of (42) into SNR of (47), and the SER of the subcarrier observed at frequency f is given by

$$\begin{aligned}&\mathrm{SER}(f) \\ &= \left(1 - \frac{1}{M}\right) \mathrm{erfc}\left(\left\{\underbrace{\frac{2(M^2-1)}{3} \cdot \frac{P_n/\zeta + S_{\hat{d}}(f)}{\alpha^2 P_{\mathrm{in}}}}_{\triangleq g(f)}\right\}^{-\frac{1}{2}}\right) \\ &= \left(1 - \frac{1}{M}\right) h\left(g\left(f\right)\right)\end{aligned} \tag{48}$$

where

$$h(x) \triangleq \mathrm{erfc}\left(x^{-\frac{1}{2}}\right). \tag{49}$$

The SER averaged over the entire bandwidth can be expressed as

$$\mathrm{SER}_{\mathrm{av}} = \int_{-\frac{1}{2}}^{\frac{1}{2}} \mathrm{SER}(f) df = \left(1 - \frac{1}{M}\right) \int_{-\frac{1}{2}}^{\frac{1}{2}} h\left(g\left(f\right)\right) df. \tag{50}$$

Since $h(x)$ is convex for $x \leq \frac{2}{3}$, we may apply Jensen's inequality to obtain

$$\mathrm{SER}_{\mathrm{av}} \geq \left(1 - \frac{1}{M}\right) h\left(\int_{-\frac{1}{2}}^{\frac{1}{2}} g\left(f\right) df\right) \tag{51}$$

where

$$\begin{aligned}\int_{-\frac{1}{2}}^{\frac{1}{2}} g\left(f\right) df &= \frac{2(M^2-1)}{3} \cdot \frac{P_n/\zeta + P_{d,\mathrm{in}}}{\alpha^2 P_{\mathrm{in}}} \\ &= \frac{2(M^2-1)}{3} \frac{1}{\mathrm{SNDR}_{\mathrm{av}}(\zeta)},\end{aligned} \tag{52}$$

provided that $g(f) \leq \frac{2}{3}$, i.e.,

$$\mathrm{SNDR}(f;\zeta) = \frac{\alpha^2 P_{\mathrm{in}}}{P_n/\zeta + S_{\hat{d}}(f)} \geq M^2 - 1. \tag{53}$$

Rearranging (51) with (49) and (52) results in (45). Also, noticing that the left hand side of (53) becomes minimal at $f = 0$, we have the condition (46). ■

We refer to the lower bound of (45) as *CAF lower bound* in what follows. It can be extended to the fading channels as

$$\mathrm{SER}_{\mathrm{LB}} = E_{\zeta}\left\{\mathrm{SER}_{\mathrm{LB}}(\zeta)\right\}, \tag{54}$$

where the expectation is over the fading coefficient $\zeta = |H|^2$. For a Rayleigh fading channel, the probability density function (pdf) of ζ is given by $f_{\zeta}(\zeta) = e^{-\zeta}$. Note that the condition (46) may not strictly hold as ζ becomes small, since the condition is equivalent to

$$\zeta \geq \left(\frac{\alpha^2}{M^2-1} - \sum_{n=1}^{\infty} C_n \xi_n(0)\right)^{-1} \frac{\eta}{\mathrm{SNR}}. \tag{55}$$

Nevertheless, the probability that the above condition holds increases as SNR increases, and thus the bound is expected to be valid even for fading channels as SNR increases.

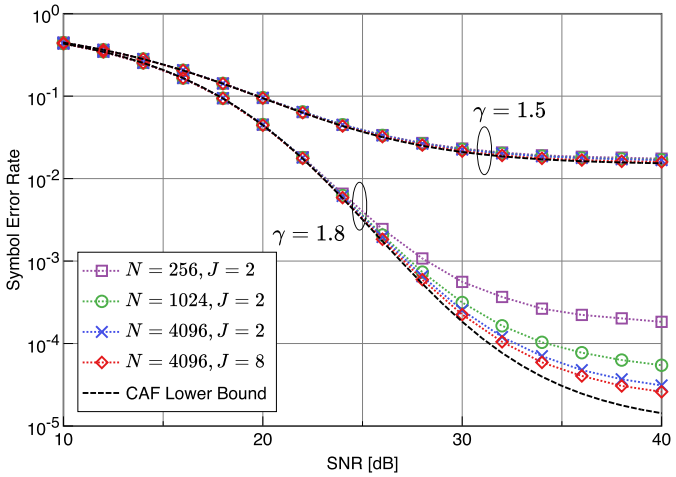

(a)

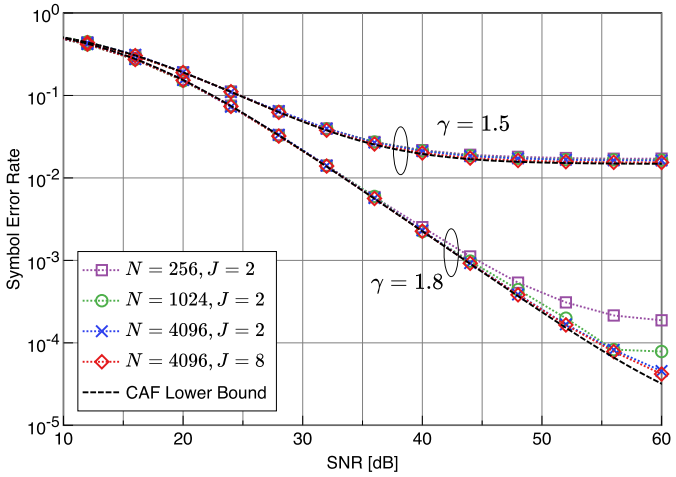

(b)

Fig. 2. Comparison of CAF lower bounds and simulated SER performances for 8-PAM over (a) AWGN channel and (b) frequency-selective Rayleigh fading channel. (Modulation is 64-QAM and the number of paths is $N_p = 4$ for fading channels.) The marks on each curve represent the simulated points.

F. Numerical Results

We compare the CAF lower bounds derived above with the SER obtained by Monte-Carlo simulations. Here, OFDM signal is modulated by 64-QAM, and we evaluate the SER performance of one-dimensional case (based on 8-PAM) without loss of generality. Both AWGN and frequency-selective channels are evaluated, where we model an N_p-path equal power i.i.d. Rayleigh fading with the CP length equal to the length of simulated channel impulse response in the latter case. For simplicity, we assume perfect channel state information (CSI), i.e., $\mathbf{H}$ is known at the receiver. The results are shown in Fig. 2 for several different values of N and J with $\gamma = 1.5$ and 1.8. In all the numerical results for the theoretical bounds, we have truncated the series corresponding to the distortion power associated with (37) at $n_{\max} = 10$. (We have numerically confirmed that increasing $n_{\max}$ more than eight would lead to negligible difference.) In the case of fading channels, only the results with $N_p = 4$ are shown, but we note that the value of N_p does not affect the SER performance of the OFDM with CAF without any distortion compensation. (Later, in Section V-C, we will observe that the performance of iterative clipping recovery schemes depends on N_p.) As the number of subcarriers N and oversampling factor J increase, the modeling of OFDM signals as a band-limited Gaussian process becomes more accurate (see also Fig. 10 in Appendix for the effect of increasing J). Therefore, we observe that the simulated SER performances approach the corresponding CAF lower bounds as N and J increase. (It appears that doubling N would contribute more effectively than doubling J to their convergence toward the corresponding bounds.) The results thus confirm that the derived bounds should well serve as a reference of the estimated OFDM performance with CAF.

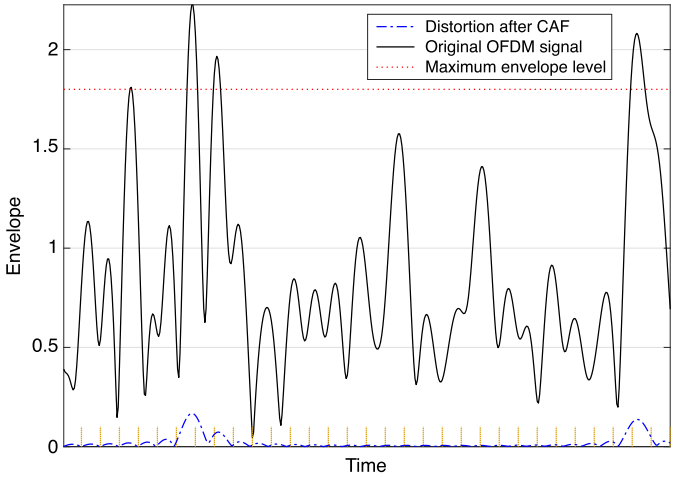

Fig. 3. Example envelopes of OFDM signal and resulting distortion after CAF with clipping ratio $\gamma = 1.8$. The average power of the OFDM envelope is normalized such that the clipping ratio corresponds to the envelope level in the figure. The vertical ticks represent the corresponding Nyquist interval T.

IV. Performance Analysis of Distortion Recovery Techniques

The previous section has demonstrated the asymptotic performance of clipped and filtered OFDM signals as the number of subcarriers increases with an ideal band-pass filtering. In this section, we extend our analysis and derive upper bounds of SNDR achieved by ideal TD and FD compensation techniques, which may serve as reference performance bounds for DAR and CNC.

A. Time-Domain Signal Reconstruction

1) Motivation: Let $z(t)$ denote a band-limited OFDM signal and $u(t)$ denote its clipped and filtered version. Let us define the distortion waveform $d(t)$ as

$$d(t) = z(t) - u(t). \tag{56}$$

Fig. 3 illustrates example envelopes of $z(t)$ and $d(t)$ generated by simulations, where $u(t)$ is obtained by CAF with $\gamma = 1.8$. We observe that the distortion waveform is a sum of the peaks that correspond to those above the clipping level. Furthermore, due to the filtering operation, each pulse caused by the clipped peak can be characterized by a sinc-like function, which indicates that the distortion caused by clipping each peak will span over a wide range in the time domain.

Consequently, some of the distortion power will be observed below the clipping threshold. On the other hand, the TD reconstruction process applies only to the missing signal above the envelope threshold. As such, even if it could ideally reconstruct all the pulses above the threshold, it may not be able to eliminate the distortion that falls below the threshold. In what follows, in order to capture the effect of the distortion after filtering, we develop a new TD analytical model for clipped and filtered OFDM signals.

2) A New Time-Domain Distortion Model: For convenience of analysis, we consider a continuous-time expression for the TD recovery process. Let $\tilde{z}(t)$ denote the received signal after ZF equalization corresponding to (10) as

$$\tilde{z}(t) = u(t) + w'(t), \tag{57}$$

where $u(t)$ is the output signal after CAF and $w'(t)$ is the AWGN term in the time domain. Based on the observation made in Fig. 3, for a given OFDM signal $z(t)$ prior to clipping, we propose to define the distortion after CAF as

$$d(t) \triangleq \sum_{l=1}^{L} \underbrace{\rho_l \operatorname{sinc}\left(\frac{t-\tau_l}{T}\right)}_{\triangleq d_l(t)}, \tag{58}$$

where $\rho_l \in \mathbb{C}$ is the distortion value associated with the lth peak to be clipped, τ_l is the corresponding time instant, L is the number of the total peaks observed, and T is the Nyquist interval. Note that the sinc function is defined as

$$\operatorname{sinc}(x) = \frac{\sin(\pi x)}{\pi x}. \tag{59}$$

To be more precise, if one takes into account the fact that the OFDM symbol period is finite, then the above sinc function should be replaced by the periodic sinc function [29]. Nevertheless, the numerical difference between them will become negligible as N increases.

In the subsequent analysis based on the mathematical model of (58), all the complex-valued peaks $\{\rho_l\}$ are assumed to be zero-mean and mutually independent, which may be a reasonable assumption as discussed in [30].

3) SNDR Analysis for Ideal TD Compensation: We consider an ideal model where the OFDM signal with CAF is reconstructed perfectly, but only in the vicinity of the positions where each signal peak envelope exceeds the threshold A. Specifically, we define the reconstructed signal as

$$\hat{z}(t) \triangleq \begin{cases} u(t) + w'(t), & \text{for} \quad |z(t)| \le A, \\ z(t) + w'(t), & \text{for} \quad |z(t)| > A, \end{cases} \tag{60}$$

where $u(t) = z(t) - d(t)$ from (56). In other words, even after ideal compensation, the distortion that falls outside the peak areas will still remain in addition to the Gaussian noise. Therefore, unlike the case with $J = 1$ (i.e., Nyquist-rate clipping without filtering) where the perfect recovery of clipping distortion might be possible, the distortion components of OFDM signal with CAF may not be completely removed.

Let $\mathcal{T}_l$ denote the bounded *interval* of its size equal to the two consecutive Nyquist intervals and its midpoint specified by the lth peak position τ_l, i.e.,

$$\mathcal{T}_l \triangleq \{t : |t - \tau_l| < T\}. \tag{61}$$

Furthermore, let $\hat{\mathcal{T}}_l$ denote the *subinterval* of $\mathcal{T}_l$, i.e., $\hat{\mathcal{T}}_l \subset \mathcal{T}_l$, where the signal envelope associated with the lth peak exceeds the threshold A, i.e.,

$$\hat{\mathcal{T}}_l \triangleq \left\{ t : |z(\tau_l)| \operatorname{sinc}\left(\frac{t-\tau_l}{T}\right) > A, \ |t - \tau_l| < T \right\}. \tag{62}$$

Since the size of $\hat{\mathcal{T}}_l$ depends on the peak amplitude $|z(\tau_l)|$, it should be regarded as a random variable. On the other hand, the size of $\mathcal{T}_l$ is constant (equal to $2T$), which is easier to deal with.

From (58) and (60), we may express the ideally reconstructed signal as

$$\hat{z}(t) = z(t) + w'(t) - \underbrace{\sum_{l=1}^{L} d_l(t)\, I_{\hat{\mathcal{T}}_l^c}(t)}_{\triangleq d_{\mathrm{TD}}(t)} \tag{63}$$

where $\mathcal{A}^c$ denotes the complementary set of $\mathcal{A}$, and $I_{\mathcal{A}}(x)$ is the indicator function that takes 1 if $x \in \mathcal{A}$ and 0 otherwise.

By the assumption that the peaks are statistically independent, we may alternatively express the average power of the in-band distortion $P_{d,\mathrm{in}}$ based on (58) as

$$\begin{aligned} P_{d,\mathrm{in}} &= E\left\{|d(t)|^2\right\} = \int_{-\infty}^{\infty} E\left\{\left|\sum_{l=1}^{L} d_l(t)\right|^2\right\} dt \\ &= \sum_{l=1}^{L} \int_{-\infty}^{\infty} E\left\{|d_l(t)|^2\right\} dt \\ &= \sum_{l=1}^{L} E\left\{|\rho_l(t)|^2\right\} \int_{-\infty}^{\infty} \operatorname{sinc}^2\left(\frac{t-\tau_l}{T}\right) dt \\ &= T \sum_{l=1}^{L} E\left\{|\rho_l(t)|^2\right\}. \end{aligned} \tag{64}$$

On the other hand, the average power of the *residual distortion* $d_{\mathrm{TD}}(t)$ in (63) may be expressed as

$$\begin{aligned} P_{d,\mathrm{TD}} &\triangleq \int_{-\infty}^{\infty} E\left\{|d_{\mathrm{TD}}(t)|^2\right\} dt = \sum_{l=1}^{L} \int_{t \in \hat{\mathcal{T}}_l^c} E\left\{|d_l(t)|^2\right\} dt \\ &\ge \sum_{l=1}^{L} \int_{t \in \mathcal{T}_l^c} E\left\{|d_l(t)|^2\right\} dt \\ &= \sum_{l=1}^{L} E\left\{|\rho_l(t)|^2\right\} \times 2 \int_{T}^{\infty} \operatorname{sinc}^2\left(\frac{t}{T}\right) dt \\ &= \sum_{l=1}^{L} E\left\{|\rho_l(t)|^2\right\} T\left(1 - 2\frac{\mathrm{Si}(2\pi)}{\pi}\right) \\ &= \underbrace{\left(1 - 2\frac{\mathrm{Si}(2\pi)}{\pi}\right)}_{\triangleq \kappa} P_{d,\mathrm{in}}, \end{aligned} \tag{65}$$

where the above inequality is due to the fact that $\hat{\mathcal{T}}_l \subset \mathcal{T}_l$ and thus $\mathcal{T}_l^c \subset \hat{\mathcal{T}}_l^c$, and $\mathrm{Si}(x)$ is the sine integral defined as

$$\mathrm{Si}(x) = \int_0^x \frac{\sin(t)}{t} dt. \tag{66}$$

Note that we can numerically calculate the parameter κ in (65) as $\kappa \approx 0.0971767$.

Consequently, from (63), the kth subcarrier can be expressed as

$$\hat{Z}_k = Z_k + \frac{W_k}{H_k} + D_{\mathrm{TD},k}, \tag{67}$$

where $D_{\mathrm{TD},k}$ is the residual distortion term $d_{\mathrm{TD}}(t)$ that falls on the kth subcarrier. As a result, similar to (43), the average SNDR can be upper bounded as

$$\begin{aligned}\mathrm{SNDR}_{\mathrm{TD}}(\zeta) &\triangleq \frac{P_{\mathrm{in}}}{P_n/\zeta + P_{d,\mathrm{TD}}} \\ &\leq \frac{P_{\mathrm{in}}}{P_n/\zeta + \kappa P_{d,\mathrm{in}}} \\ &= \frac{1}{\frac{\eta}{\zeta}\mathrm{SNR}^{-1} + \kappa \sum_{n=1}^{\infty} C_n \delta_{n,\mathrm{in}}} \\ &\triangleq \mathrm{SNDR}_{\mathrm{TD,UB}}(\zeta). \end{aligned} \tag{68}$$

The corresponding SER lower bound can be obtained by substituting $\mathrm{SNDR}_{\mathrm{TD,UB}}(\zeta)$ of (68) into $\mathrm{SNDR}_{\mathrm{av}}(\zeta)$ of (45), which may serve as a reference for TD reconstruction schemes. We refer to this SER bound as *TD lower bound* in what follows.

B. Frequency-Domain Signal Reconstruction

Next, we discuss the achievable performance when the perfect FD distortion cancellation can be performed at the receiver for CAF. By assuming that all the distortion terms are correctly canceled, the received signal of (11) will be replaced by

$$\tilde{\mathbf{Z}}/\alpha = \mathbf{Z} + \mathbf{W}'/\alpha, \tag{69}$$

and thus the SNDR upper bound of the subcarrier with its squared channel coefficient $\zeta = |H|^2$ is expressed, similar to (43), as

$$\mathrm{SNDR}_{\mathrm{FD}}(\zeta) = \frac{\alpha^2 P_{\mathrm{in}}}{P_n/\zeta} = \frac{\alpha^2}{\eta}\zeta\,\mathrm{SNR}. \tag{70}$$

Similar to the TD reconstruction case, the SER lower bound can be obtained by substituting $\mathrm{SNDR}_{\mathrm{FD}}(\zeta)$ of (70) into $\mathrm{SNDR}_{\mathrm{av}}(\zeta)$ of (45). We refer to the corresponding SER lower bound as *FD lower bound* in what follows, which may serve as a lower SER limit in the case of CNC.

From (70), we observe that there is always a penalty in terms of SNR by a factor of $\Delta \triangleq \alpha^2/\eta$ for the case of FD distortion cancellation compared to the unclipped case even if the distortion is completely canceled. This SNR reduction factor can be seen from (39) as

$$\Delta = \frac{\alpha^2}{\alpha^2 + \sum_{n=1}^{\infty} C_n \delta_{n,\mathrm{in}}}. \tag{71}$$

The above factor Δ is plotted in Fig. 4 as a function of γ, where the distortion power is calculated based on the series expression of (37) truncated at $n_{\max} = 10$. We observe that the penalty is less than 0.2 dB for $\gamma \geq 1$ and it becomes negligible as γ increases.

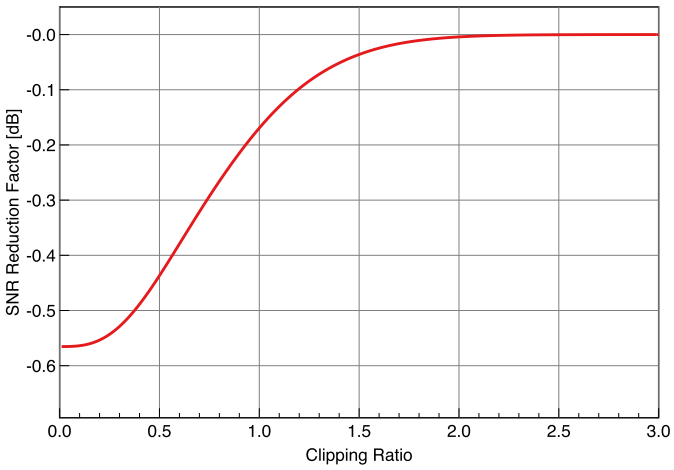

Fig. 4. The SNR reduction factor Δ due to CAF with FD distortion cancellation as a function of clipping ratio γ.

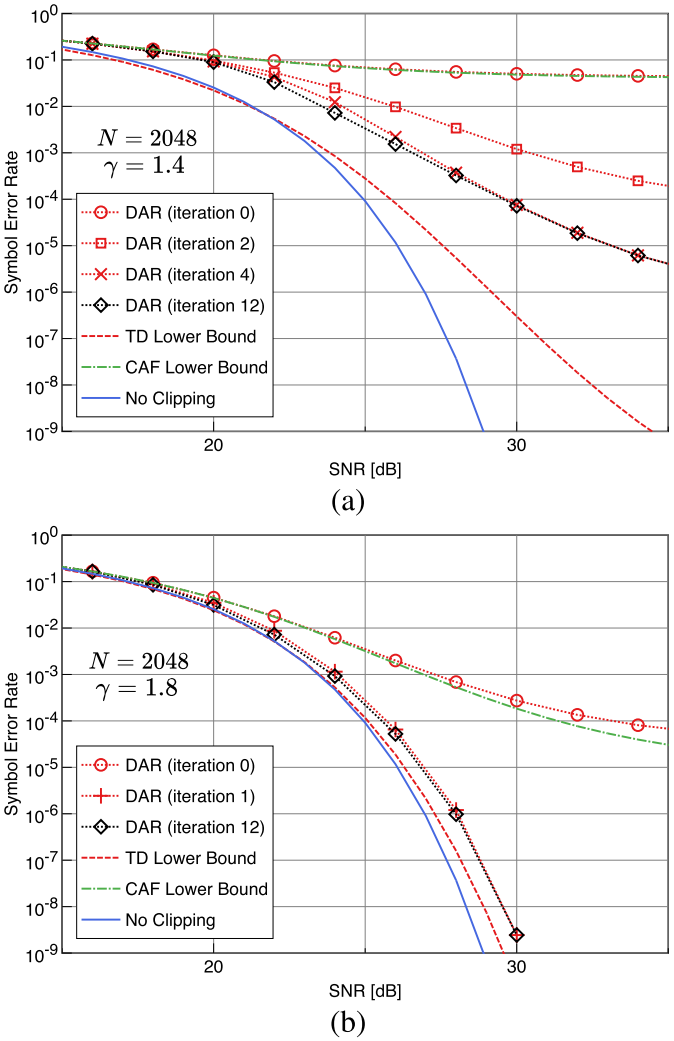

Fig. 5. Comparison of SER performances achieved by DAR for 2048-subcarrier OFDM signals over an AWGN channel where CAF is performed with (a) $\gamma = 1.4$ and (b) $\gamma = 1.8$. The marks on each curve represent the simulated points.

V. Simulation Results

In this section, we evaluate the theoretical SER lower bounds of TD signal recovery and FD distortion cancellation

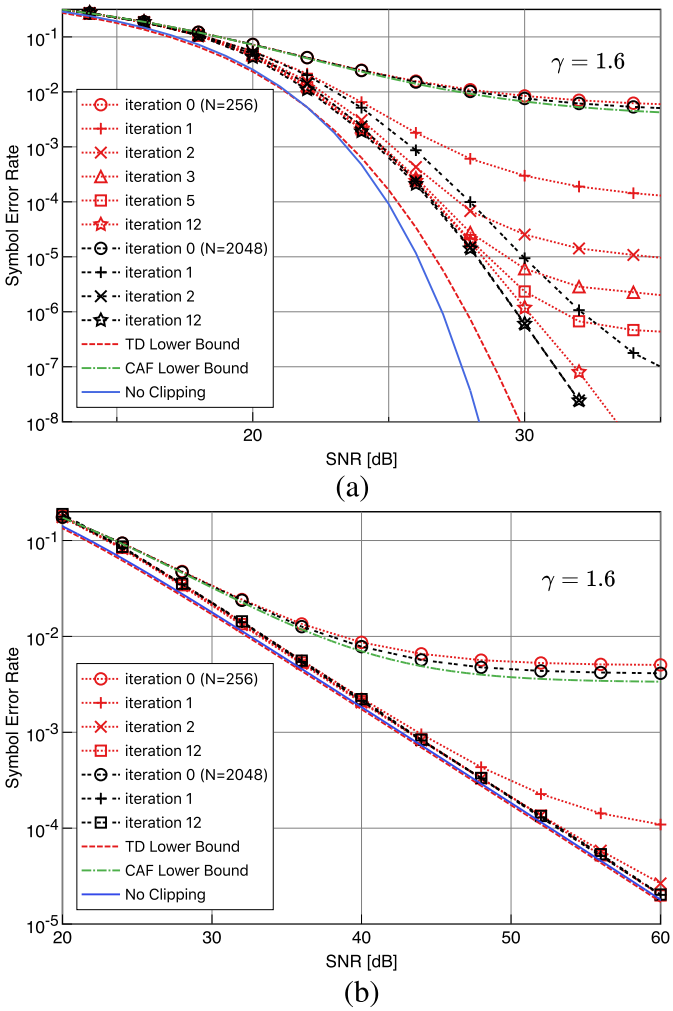

Fig. 6. Comparison of SER performances achieved by DAR for 256 and 2048-subcarrier OFDM signals over (a) AWGN channel and (b) frequency-selective Rayleigh fading channel, where CAF is performed with $\gamma = 1.6$. The marks on each curve represent the simulated points.

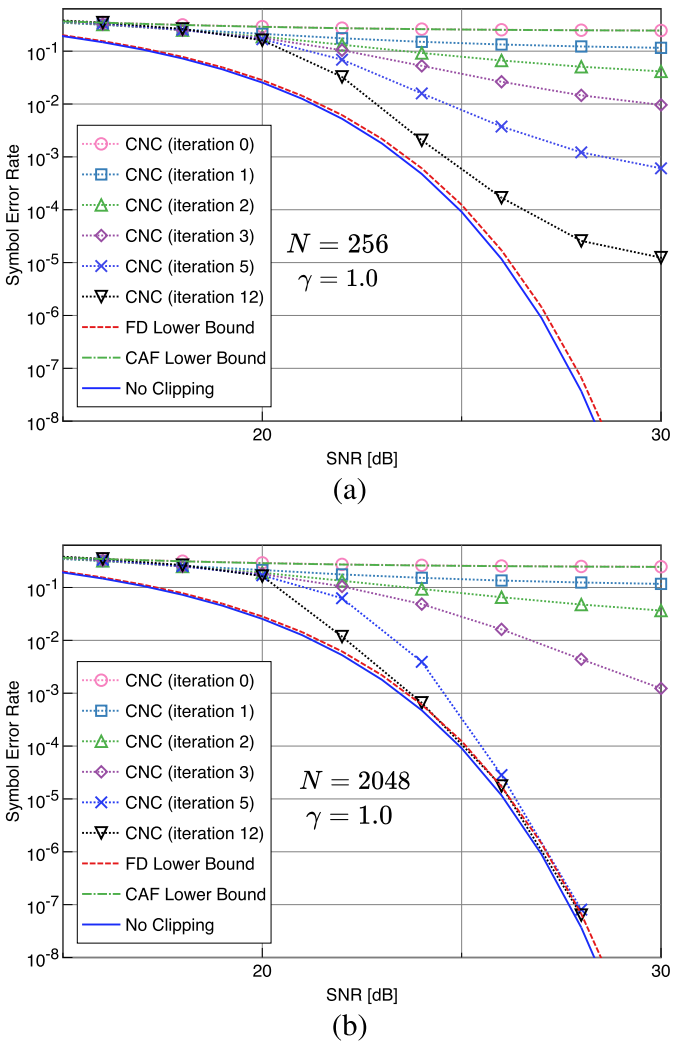

Fig. 7. Comparison of SER performances achieved by CNC for OFDM signals with (a) $N = 256$ and (b) $N = 2048$, both over an AWGN channel, where CAF is performed with $\gamma = 1.0$. The marks on each curve represent the simulated points. The SNR reduction factor is -0.17 dB in this case.

schemes, and compare them with the corresponding simulation results based on DAR and CNC described in Section II. Each subcarrier is modulated by 64-QAM, and we evaluate the SER with 8-PAM (i.e., $M = 8$) throughout this section. Also, the oversampling factor is set as $J = 2$. In the case of frequency-selective fading channels, we assume an i.i.d. equal power Rayleigh fading channel model with $N_p = 4$ paths, unless stated otherwise. The CP length is chosen to be equal to the delay spread such that the ISI is negligible, and the CSI $\mathbf{H}$ is assumed to be available at the receiver.

A. SER Performance of TD Recovery Schemes

Figs. 5(a) and (b) show the SER performances of DAR applied to 2048-subcarrier OFDM signals after CAF with $\gamma = 1.4$ and $\gamma = 1.8$, respectively, with the maximum iterations $I_{\max} = 12$. Also shown in the figures are the corresponding theoretical references, i.e., the TD lower bound based on (68), the CAF lower bound of (45), and the ideal SER performance without CAF. From Fig. 5(a), we observe that in the case of $\gamma = 1.4$, the performance almost saturates after iterations of $i = 4$. (Note that the performance with $i = 0$ corresponds to the case without any compensation and thus should be bounded by the CAF lower bound.) We also observe that the gap of the achievable performance with $i = I_{\max} = 12$ and the TD lower bound is still noticeable. In the case of $\gamma = 1.8$, we observe from Fig. 5(b) that the performance almost saturates even with the first iteration, and the gap from the TD lower bound becomes smaller. From these results, we clearly observe that DAR cannot achieve the performance comparable to the case without CAF due to the residual distortion as discussed in the previous section.

Note that in the case of Fig. 5(a), we also observe that the SER corresponding to the TD lower bound is even lower than that without clipping in the low SNR region. This is due to the fact that clipping of OFDM signal leads to reduction of the transmit power. Therefore, if the OFDM signal were successfully reconstructed from its clipped and filtered signal, it would improve the SER performance even over the unclipped case. In practice, however, successful reconstruction cannot be achieved in such low SNR region by simulation with DAR, thus leading to a significant gap from the corresponding theoretical bound.

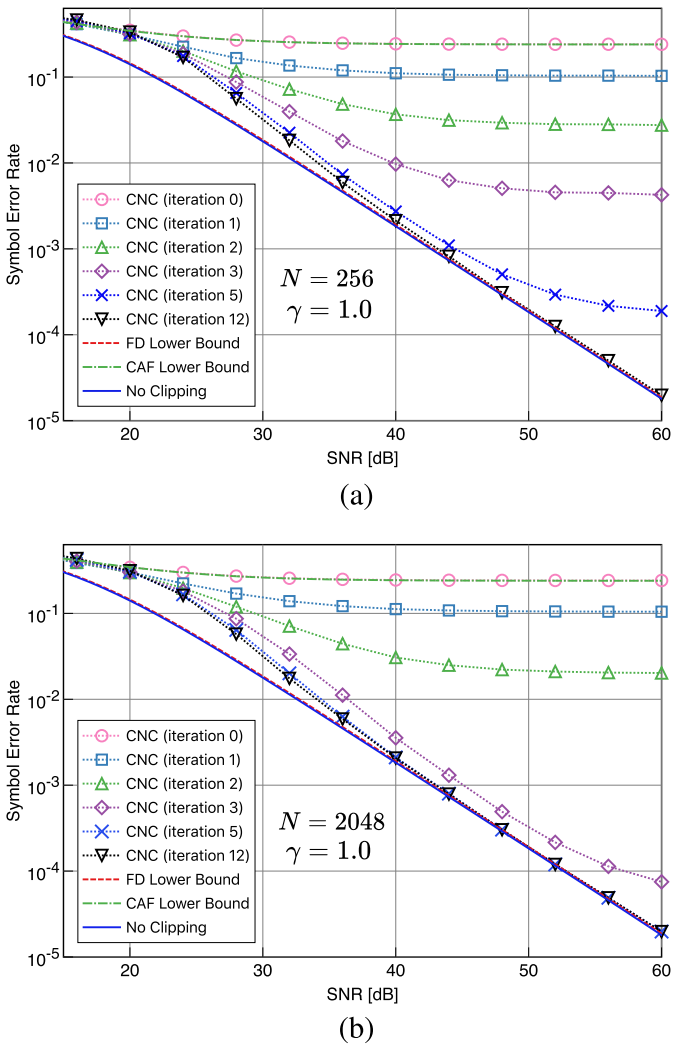

Fig. 8. Comparison of SER performances achieved by CNC for OFDM signals with (a) $N = 256$ and (b) $N = 2048$ both over frequency-selective Rayleigh fading channel, where CAF is performed with $\gamma = 1.0$. The marks on each curve represent the simulated points. The SNR reduction factor in this case is -0.17 dB.

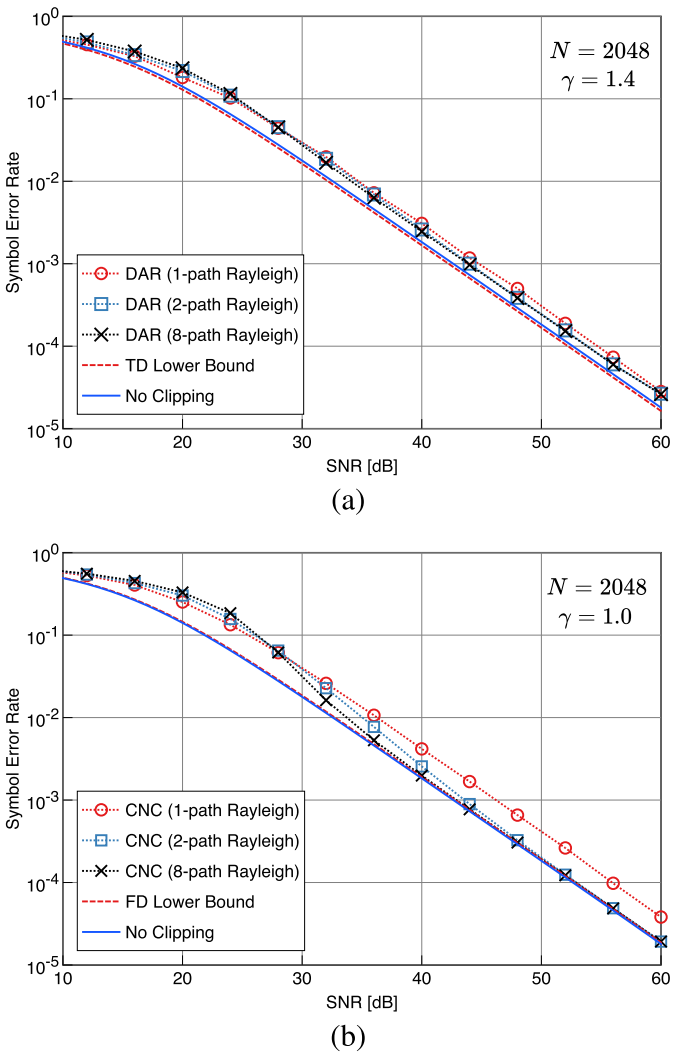

Fig. 9. Comparison of SER performances achieved by the two recovery schemes over frequency-selective fading channels with a different number of paths N_p. (a) DAR with $\gamma = 1.4$. (b) CNC with $\gamma = 1.0$, both with $I_{\max} = 5$. The marks on each curve represent the simulated points.

Next, in Figs. 6(a) and (b), we compare the DAR performances with $\gamma = 1.6$ over AWGN and frequency-selective fading channels, respectively. For each figure, we compare the two different subcarrier numbers: $N = 256$ and 2048. From these results, for both channels we observe that as the number of subcarriers increases, the performance improvement per iteration becomes more significant until its saturation. Furthermore, from Fig. 6(b), we also observe that the relative gap from the case without clipping becomes smaller for Rayleigh fading channels. This stems from the fact that the negative effect of signal fluctuation caused by Rayleigh fading on SER is more severe than that of residual distortion.

B. SER Performance of FD Distortion Cancellation Schemes

In Figs. 7(a) and (b), we show the SER performances of OFDM with $N = 256$ and 2048, respectively, where CAF is applied with $\gamma = 1.0$ and the receiver employs CNC with $I_{\max} = 12$. Also shown in the figures are the corresponding theoretical references, i.e., the FD lower bound based on (70), the CAF lower bound of (45), and the ideal SER performance without CAF. Note that SNR reduction factor is about -0.17 dB according to Fig. 4.

From Fig. 7(a), we observe that even after $i = I_{\max} = 12$ iterations, there is a performance gap from the FD lower bound based on the ideal distortion cancellation. Nevertheless, as we increase the number of subcarriers, it eventually converges to the lower bound as observed in Fig. 7(b), especially in the high SNR region. Therefore, we may conclude that increasing subcarriers will help improve the performance of clipping recovery techniques in general. We conjecture that increasing N not only contributes to make the OFDM signal *more Gaussian*, which justifies the use of the model based on Bussgang's theorem for the FD approaches, but also helps reducing the variance of error in estimating clipped signal or distortion components as the distortion induced in the time domain clipping is shared by all the subcarriers.

Figs. 8(a) and (b) show the SER performances of the same OFDM system over Rayleigh fading channels. Similar to the case with DAR, the gap from the FD lower bound is negligible even for the case with $N = 256$, as the effect of signal fading becomes dominant compared to the residual distortion that has not been canceled by CNC. Furthermore, comparing the two figures, we clearly observe that increasing the number of subcarriers may accelerate the performance convergence to the theoretical limit.

Comparing the performances of CNC with DAR, it is clear that CNC is more effective if CAF with similar clipping ratio is applied at the transmitter, despite its lower complexity compared to DAR.

C. SER Performance Comparison Over Frequency Selective Rayleigh Fading Channels

Finally, we compare the performances of DAR and CNC with several different cases with respect to the numbers of paths in an i.i.d. equal power Rayleigh fading channel. Figs. 9(a) and (b) show the SER results of 2048-subcarrier OFDM signals in the cases of DAR for CAF with $\gamma = 1.4$ and CNC for CAF with $\gamma = 1.0$, respectively, where the number of paths N_p is chosen from $\{1, 2, 8\}$ and $I_{\max} = 5$. (Note that due to the difference in clipping ratio applied to the two results, the effect of distortion should be more dominant for CNC.) It is interesting to observe that, for the case of $N_p = 1$, there is some degradation in achievable SER in high SNR region for both cases. We particularly observe from Fig. 9(b) that the convergence of SER to the theoretical limit becomes faster as the number of paths increases in the case of CNC. This is because the frequency diversity effect can be partially exploited upon estimation of distortion terms even for the uncoded cases. Note that since the final decision is made on symbol by symbol basis, the diversity effect cannot be exploited for the SER performance, which is in contrast to the maximum-likelihood-based detectors (e.g., [9], [10]). Similar to the conventional OFDM systems, combination with channel coding may further improve the performance as it helps achieving the diversity effect offered by the frequency-selective nature of fading channels. The detailed analysis for the coded OFDM cases is left as future work.

VI. Conclusion

In this work, we have analyzed the performance of CAF on OFDM signals with emphasis on the TD and FD iterative clipping compensation techniques applied at the receiver. We have derived a closed-form SDR expression for OFDM with CAF based on the conventional analysis of band-limited complex Gaussian signals with nonlinearity. We also introduced a new time-domain distortion model, based on which we have analyzed the SNDR upper bound for the case of CAF with ideal TD recovery technique. We have also derived the achievable performance loss over unclipped system in the case of ideal FD distortion cancellation approach, which becomes negligibly small as the clipping ratio increases. We have revealed that in the case of CAF, the TD approach suffers from the unrecoverable distortion that falls below the clipping threshold, and thus the achievable performance will be degraded. Our simulation results based CNC (for a practical FD approach) and DAR (for a practical TD approach) have confirmed the validity of our theoretical modeling and analysis. Therefore, if we compare CNC and DAR which share almost the same complexity, CNC will be preferable compared to DAR both over AWGN and Rayleigh fading channels in the case of CAF. In other words, more complex additional recovery structures that precisely capture the property of the band-limited distortion pulses should be incorporated in its TD reconstruction process.

Appendix

We derive the average SDR expression based on the approach proposed in [4], which in general leads to a more complex formula than the one derived in Section III.

We first note that the discrete-frequency (subcarrier-wise) power spectrum of the input OFDM symbol modulated with i.i.d. QAM symbols can be expressed from (2) as

$$\mathbf{P}_Z = P_{\text{in}} \left(\mathbf{1}_N, \mathbf{0}_{(J-1)N} \right), \tag{72}$$

where $\mathbf{1}_n$ denotes the all-one vector of length n. The corresponding discrete-time autocorrelation function is expressed as $\mathbf{R}_Z = (R_{Z,0}, R_{Z,1}, \cdots, R_{Z,JN-1})$ defined for $m \in \{0, 1, \cdots, JN-1\}$ where

$$R_{Z,m} = \sum_{k=0}^{N-1} P_{\text{in}} e^{j2\pi \frac{k}{JN} m}. \tag{73}$$

Let us introduce a frequency offset to make the power spectrum symmetric at the origin, and let $R_{Z',m}$ denote the resulting autocorrelation function, which is expressed as [4]

$$R_{Z',m} = e^{j\varphi_{J,m}} R_{Z,m}, \tag{74}$$

where $\varphi_{J,m} \triangleq \frac{m(1-N)}{JN}\pi$. The corresponding correlation coefficient can be expressed as

$$\rho_{Z',m} \triangleq \frac{R_{Z',m}}{R_{Z',0}} = \begin{cases} 1, & m = 0, \\ \dfrac{1}{N} \dfrac{\sin\left(\pi \frac{m}{J}\right)}{\sin\left(\pi \frac{m}{JN}\right)}, & 0 < m < JN. \end{cases} \tag{75}$$

Note that $\rho_{Z',m}$ satisfies the symmetric property that $\rho_{Z',m} = -\rho_{Z',JN-m}$ for $0 < m \leq \frac{JN}{2} - 1$. In the case of soft-envelope limiter, let $\mathbf{R}_{\tilde{Z}'}$ denote a vector representing the autocorrelation of the clipped signal, whose mth element can be expressed from [4, eq.(B9)] as

$$R_{\tilde{Z}',m} = N P_{\text{out}} L_m \tag{76}$$

with $L_0 \triangleq 1$ and for $m > 0$

$$\begin{aligned} L_m &\triangleq \frac{\rho_{Z',m}(1-\rho_{Z',m}^2)^2}{1-e^{-\gamma^2}} \sum_{n=0}^{\infty} \rho_{Z',m}^{2n}(n+1) \\ &\quad \times \left\{ \frac{\gamma}{\sqrt{1-\rho_{Z',m}^2}} \frac{\Gamma\left(n+\frac{3}{2}\right)}{\Gamma(n+2)} \left[1 - P\left(n+\frac{3}{2}, \frac{\gamma^2}{1-\rho_{Z',m}^2} \right) \right] \right. \\ &\quad \left. + P\left(n+2, \frac{\gamma^2}{1-\rho_{Z',m}^2} \right) \right\}^2, \end{aligned} \tag{77}$$

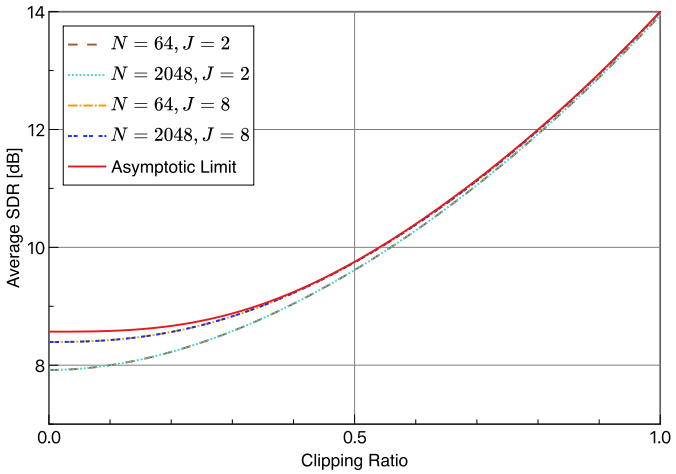

Fig. 10. Comparison of the average SDR based on (86) and its asymptotic limit (40).

where $\Gamma(a)$ is the gamma function and $P(a,x)$ is the incomplete gamma function defined as

$$P(a,x) \triangleq \frac{1}{\Gamma(a)} \int_0^x e^{-t} t^{a-1} dt. \tag{78}$$

Let $\mathbf{R}_{\tilde{Z}}$ denote a vector after the inverse frequency offset, whose mth element is

$$R_{\tilde{Z},m} = e^{-j\varphi_{J,m}} R_{\tilde{Z}',m}. \tag{79}$$

The discrete-frequency power spectrum corresponding to the output is given by

$$\mathbf{P}_{\tilde{Z}} = \left(P_{\tilde{Z},0}, P_{\tilde{Z},1}, \cdots, P_{\tilde{Z},JN-1} \right), \tag{80}$$

where

$$P_{\tilde{Z},k} = \frac{1}{JN} \sum_{m=0}^{JN-1} R_{\tilde{Z},m} e^{-j2\pi \frac{k}{JN} m}. \tag{81}$$

Under the assumption that N is an even integer, substituting (79) into (81) and noticing the symmetry $R_{\tilde{Z}',m} = -R_{\tilde{Z}',JN-m}$, we obtain

$$P_{\tilde{Z},k} = \frac{P_{\text{out}}}{J} \left\{ 1 + 2 \sum_{m=1}^{\frac{JN}{2}-1} \cos\left(\frac{\pi}{JN} m \left(N - 1 - 2k \right) \right) L_m \right\}. \tag{82}$$

The SDR on the kth subcarrier is then expressed as

$$\text{SDR}_k = \frac{\alpha^2 P_{\text{in}}}{P_{\tilde{Z},k} - \alpha^2 P_{\text{in}}}. \tag{83}$$

Analogous to (40), we may define the average SDR as

$$\text{SDR}_{\text{av}} \triangleq \frac{\alpha^2 P_{\text{in}}}{\frac{1}{N} \sum_{k=0}^{N-1} \left\{ P_{\tilde{Z},k} - \alpha^2 P_{\text{in}} \right\}}. \tag{84}$$

Since

$$\sum_{k=0}^{N-1} P_{\tilde{Z},k} = \frac{P_{\text{out}}}{J} \left\{ N + 2 \sum_{m=1}^{\frac{JN}{2}-1} \frac{\sin\left(\frac{m\pi}{J}\right)}{\sin\left(\frac{m\pi}{JN}\right)} L_m \right\}, \tag{85}$$

we have

$$\text{SDR}_{\text{av}} = \frac{K_\gamma}{\frac{1}{J} \left\{ 1 + \frac{2}{N} \sum_{m=1}^{\frac{JN}{2}-1} \frac{\sin\left(\frac{m\pi}{J}\right)}{\sin\left(\frac{m\pi}{JN}\right)} L_m \right\} - K_\gamma}, \tag{86}$$

where $K_\gamma \triangleq \alpha^2/(1 - e^{-\gamma^2})$ as defined in [4].

In Fig. 10, we compare the numerical results based on (86) for several values of N and J, as well as the asymptotic limit (40) derived in Section III with the series truncated at $n_{\max} = 10$. It is observed that increasing N in (86) does not make any noticeable difference as the theoretical model already assumes Gaussian signaling. As expected, however, by increasing J we observe that the curves approach the asymptotic limit.

REFERENCES

[1] S. H. Han and J. H. Lee, "An overview of peak-to-average power ratio reduction techniques for multicarrier transmission," *IEEE Wireless Commun.*, vol. 12, no. 2, pp. 56–65, Apr. 2005.
[2] T. Jiang and Y. Wu, "An overview: Peak-to-average power ratio reduction techniques for OFDM signals," *IEEE Trans. Broadcast.*, vol. 54, no. 2, pp. 257–268, Jun. 2008.
[3] X. Li and L. J. Cimini, "Effects of clipping and filtering on the performance of OFDM," *IEEE Commun. Lett.*, vol. 2, no. 5, pp. 131–133, May 1998.
[4] H. Ochiai and H. Imai, "Performance analysis of deliberately clipped OFDM signals," *IEEE Trans. Commun.*, vol. 50, no. 1, pp. 89–101, Jan. 2002.
[5] H. Ochiai and H. Imai, "Performance of the deliberate clipping with adaptive symbol selection for strictly band-limited OFDM systems," *IEEE J. Sel. Areas Commun.*, vol. 18, no. 11, pp. 2270–2277, Nov. 2000.
[6] T. May and H. Rohling, "Reducing the peak-to-average power ratio in OFDM radio transmission systems," in *Proc. 48th IEEE Veh. Technol. Conf. Pathway Global Wireless Revolution (VTC)*, Ottawa, ON, Canada, vol. 3, May 1998, pp. 2474–2478.
[7] J. Song and H. Ochiai, "Performance analysis for OFDM signals with peak cancellation," *IEEE Trans. Commun.*, vol. 64, no. 1, pp. 261–270, Jan. 2016.
[8] J. Tellado, L. M. C. Hoo, and J. M. Cioffi, "Maximum-likelihood detection of nonlinearly distorted multicarrier symbols by iterative decoding," *IEEE Trans. Commun.*, vol. 51, no. 2, pp. 218–228, Feb. 2003.
[9] H. Ochiai, "Performance of optimal and suboptimal detection for uncoded OFDM system with deliberate clipping and filtering," in *Proc. IEEE GLOBECOM*, San Francisco, CA, USA, Dec. 2003, pp. 1618–1622.
[10] F. Peng and W. E. Ryan, "MLSD bounds and receiver designs for clipped OFDM channels," *IEEE Trans. Wireless Commun.*, vol. 7, no. 9, pp. 3568–3578, Sep. 2008.
[11] D. Kim and G. L. Stuber, "Clipping noise mitigation for OFDM by decision-aided reconstruction," *IEEE Commun. Lett.*, vol. 3, no. 1, pp. 4–6, Jan. 1999.
[12] H. Chen and A. M. Haimovich, "Iterative estimation and cancellation of clipping noise for OFDM signals," *IEEE Commun. Lett.*, vol. 7, no. 7, pp. 305–307, Jul. 2003.
[13] H. E. Rowe, "Memoryless nonlinearities with Gaussian inputs: Elementary results," *Bell Syst. Tech. J.*, vol. 61, no. 7, pp. 1519–1526, Sep. 1982.
[14] E. B. Al-Safadi and T. Y. Al-Naffouri, "Peak reduction and clipping mitigation in OFDM by augmented compressive sensing," *IEEE Trans. Signal Process.*, vol. 60, no. 7, pp. 3834–3839, Jul. 2012.
[15] K.-H. Kim, H. Park, J.-S. No, H. Chung, and D.-J. Shin, "Clipping noise cancelation for OFDM systems using reliable observations based on compressed sensing," *IEEE Trans. Broadcast.*, vol. 61, no. 1, pp. 111–118, Mar. 2015.
[16] T. Liu, S. Jin, C.-K. Wen, and X. You, "OFDM-clipped signal recovery and learning using Gaussian mixture GTurbo approach," *IEEE Wireless Commun. Lett.*, vol. 8, no. 6, pp. 1533–1536, Dec. 2019.
[17] W. Jiang, X. Kuai, X. Yuan, W. Liu, and Z. Song, "Sparsity-learning-based iterative compensation for filtered-OFDM with clipping," *IEEE Commun. Lett.*, vol. 24, no. 11, pp. 2483–2487, Nov. 2020.
[18] M. Colas, G. Gelle, and D. Declercq, "Turbo decision aided receivers for clipping noise mitigation in coded OFDM," *EURASIP J. Wireless Commun. Netw.*, vol. 2008, no. 1, pp. 1–10, Dec. 2007.

[19] U.-K. Kwon, D. Kim, and G.-H. Im, "Amplitude clipping and iterative reconstruction of MIMO-OFDM signals with optimum equalization," *IEEE Trans. Wireless Commun.*, vol. 8, no. 1, pp. 268–277, Jan. 2009.
[20] J. Tong, L. Ping, Z. Zhang, and V. K. Bhargava, "Iterative soft compensation for OFDM systems with clipping and superposition coded modulation," *IEEE Trans. Commun.*, vol. 58, no. 10, pp. 2861–2870, Oct. 2010.
[21] S. Liang, J. Tong, and L. Ping, "On iterative compensation of clipping distortion in OFDM systems," *IEEE Wireless Commun. Lett.*, vol. 8, no. 2, pp. 436–439, Apr. 2019.
[22] N. Blachman, "The output signals and noise from a nonlinearity with amplitude-dependent phase shift," *IEEE Trans. Inf. Theory*, vol. IT-25, no. 1, pp. 77–79, Jan. 1979.
[23] P. Banelli and S. Cacopardi, "Theoretical analysis and performance of OFDM signals in nonlinear AWGN channels," *IEEE Trans. Commun.*, vol. 48, no. 3, pp. 430–441, Mar. 2000.
[24] T. Lee and H. Ochiai, "Characterization of power spectral density for nonlinearly amplified OFDM signals based on cross-correlation coefficient," *EURASIP J. Wireless Commun. Netw.*, vol. 2014, no. 1, pp. 1–15, Dec. 2014.
[25] M. Abramowitz and I. A. Stegun, Eds., *Handbook of Mathematical Functions*. New York, NY, USA: Dover, 1965.
[26] D. Dardari, "Joint clip and quantization effects characterization in OFDM receivers," *IEEE Trans. Circuits Syst. I, Reg. Papers*, vol. 53, no. 8, pp. 1741–1748, Aug. 2006.
[27] D. R. Morgan, "Finite limiting effects for a band-limited Gaussian random process with applications to A/D conversion," *IEEE Trans. Acoust., Speech, Signal Process.*, vol. ASSP-36, no. 7, pp. 1011–1016, Jul. 1988.
[28] J. G. Proakis and M. Salehi, *Digital Communications*, 5th ed. Boston, MA, USA: McGraw-Hill, 2008.
[29] H. Ochiai, "High-order moments and Gaussianity of single-carrier and OFDM signals," *IEEE Trans. Commun.*, vol. 63, no. 12, pp. 4964–4976, Dec. 2015.
[30] H. Ochiai and H. Imai, "On the distribution of the peak-to-average power ratio in OFDM signals," *IEEE Trans. Commun.*, vol. 49, no. 2, pp. 282–289, Feb. 2001.

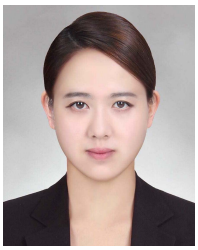

Ying Sun received the B.E. degree in electrical engineering from the Changchun University of Technology, Changchun, China, in 2012, and the M.E. degree in communication engineering from Ewha Womans University, Seoul, South Korea, in 2016. She is currently pursuing the Ph.D. degree in communication engineering with Yokohama National University, Yokohama, Japan. Her research interest includes signal processing techniques in OFDM systems.

Hideki Ochiai (Senior Member, IEEE) received the Ph.D. degree in information and communication engineering from The University of Tokyo, Tokyo, Japan, in 2001.

From 2001 to 2003, he was a Research Associate with the University of Electro-Communications, Tokyo. Since April 2003, he has been with Yokohama National University, Yokohama, Japan, where he is currently a Professor. From 2003 to 2004, he was a Visiting Scientist with Harvard University, Cambridge, MA, USA. From 2019 to 2020, he was a Visiting Professor with the University of Waterloo, Waterloo, ON, Canada, and a Visiting Fellow with Princeton University, Princeton, NJ, USA. He served as an Editor for the IEEE TRANSACTIONS ON WIRELESS COMMUNICATIONS from 2007 to 2011 and for the IEEE WIRELESS COMMUNICATIONS LETTERS from 2011 to 2016.